INFECTION AND IMMUNITY, Oct. 2007, p. 4743–4753 Vol. 75, No. 10
0019-9567/07/$08.00+0 doi:10.1128/IAI.00687-07

Dynamics of *Neisseria gonorrhoeae* Attachment: Microcolony Development, Cortical Plaque Formation, and Cytoprotection▽§

Dustin L. Higashi,[1]† Shaun W. Lee,[1]‡ Aurelie Snyder,[2] Nathan J. Weyand,[1]† Antony Bakke,[3] and Magdalene So[1]*

Department of Molecular Microbiology and Immunology,[1] Microscopy Core Facility,[2] and Department of Pathology,[3] Oregon Health and Science University, 3181 SW Sam Jackson Park Rd., Portland, Oregon 97239

Received 18 May 2007/Returned for modification 16 July 2007/Accepted 24 July 2007

***Neisseria gonorrhoeae* is the bacterium that causes gonorrhea, a major sexually transmitted disease and a significant cofactor for human immunodeficiency virus transmission. The retractile *N. gonorrhoeae* type IV pilus (Tfp) mediates twitching motility and attachment. Using live-cell microscopy, we reveal for the first time the dynamics of twitching motility by *N. gonorrhoeae* in its natural environment, human epithelial cells. Bacteria aggregate into microcolonies on the cell surface and induce a massive remodeling of the microvillus architecture. Surprisingly, the microcolonies are motile, and they fuse to form progressively larger structures that undergo rapid reorganization, suggesting that bacteria communicate with each other during infection. As reported, actin plaques form beneath microcolonies. Here, we show that cortical plaques comigrate with motile microcolonies. These activities are dependent on *pilT*, the Tfp retraction locus. Cultures infected with a *pilT* mutant have significantly higher numbers of apoptotic cells than cultures infected with the wild-type strain. Inducing *pilT* expression with isopropyl-β-D-thiogalactopyranoside partially rescues cells from infection-induced apoptosis, demonstrating that Tfp retraction is intrinsically cytoprotective for the host. Tfp-mediated attachment is therefore a continuum of microcolony motility and force stimulation of host cell signaling, leading to a cytoprotective effect.**

Type IV pili (Tfp) are filamentous appendages expressed by a wide range of bacteria, including *Synechocystis* spp., *Pseudomonas aeruginosa*, *Myxococcus xanthus*, *Xylella fastidiosa*, *Clostridium perfringens*, enterohaemorrhagic and enteropathogenic *Escherichia coli*, *Neisseria meningitidis*, and *Neisseria gonorrhoeae* (29, 32, 37, 50, 54, 56, 61). The Tfp of several of these bacteria are known to retract, and retraction underlies twitching motility, DNA uptake, phage sensitivity, and social behavior, such as fruiting-body and biofilm formation.

N. gonorrhoeae, the bacterium that causes gonorrhea, expresses multiple nonpolar retractile Tfp that promote attachment to epithelial cells (38). Retraction requires the ATPase PilT, which is proposed to disassemble the Tfp fiber (2, 13, 15). *N. gonorrhoeae pilT* null mutants express nonretractile Tfp (38, 60). Cycles of Tfp extension, substrate tethering, and retraction enable *N. gonorrhoeae* to crawl on a glass coverslip or agar surface (twitching motility) (34). Twitching motility on epithelial cells has not been studied. Understanding *N. gonorrhoeae* motility behavior in this environment is important, as the bacterium infects only humans and cannot survive outside the human body.

Mechanical forces of 50 to 100 pN are generated by the retraction of a Tfp fiber (24, 38). Thus, Tfp retraction allows *N. gonorrhoeae* to pull and exert physical stress on its substrate. Tfp retraction induces a number of responses in the infected epithelial cell. It triggers Ca^{2+} and stress kinase signaling, cytoskeletal rearrangements, and cortical plaque formation and regulates epithelial gene expression (3, 17, 23, 33). In turn, these host responses enhance *N. gonorrhoeae* aggregative behavior, promote bacterial invasion, and dampen apoptosis signaling (17, 23). Eucaryotic cells respond similarly when they experience artificial forces of ≤100 pN (12, 46, 58).

Cell culture studies have revealed key morphological features of Tfp-mediated attachment (11, 30, 31, 35, 37, 40, 52). Tfp-expressing *N. gonorrhoeae* has been observed to attach to cells as individual diplococci and as microcolonies and to induce dramatic changes in the epithelial cell cortex at the attachment site (31, 36, 52). These studies gave rise to the current notion that attachment proceeds in distinct stages involving an initial loose attachment, followed by microcolony formation and microvillus deformation and subsequent microcolony dispersal and intimate attachment.

Because these cell culture studies were performed on fixed cell preparations taken from a few infection time points, they provide only a limited view of Tfp-based attachment. For instance, there is no dynamic information on bacterium-bacterium and bacterium-host interactions. Moreover, it is unclear how attachment, which is currently understood to progress in a stepwise fashion, fits within the framework of bacterial twitching motility and host cell signaling. Using live-cell microscopy, we provide the first movies of *N. gonorrhoeae* attaching to human epithelial cells. We demonstrate that Tfp-mediated attachment does not proceed in distinct stages. Rather, it can best be characterized as a continuum of microcolony motion

* Corresponding author. Present address: Department of Immunobiology and BIO5 Institute, University of Arizona, 1657 E. Helen St., Tucson, AZ 85721. Phone: (520) 626-3097. Fax: (520) 626-4824. E-mail: somaggie@email.arizona.edu.

† Present address: Department of Immunobiology and BIO5 Institute, University of Arizona, Tucson, AZ 85718.

‡ Present address: Department of Pharmacology, University of California, San Diego, La Jolla, CA 92093-0721.

§ Supplemental material for this article may be found at http://iai.asm.org/.

▽ Published ahead of print on 6 August 2007.

and fusion and force stimulation of host cell signaling. We reported previously that Tfp retraction dampens infection-induced apoptosis signaling, as judged by poly(ADP) ribose polymerase (PARP) and caspase 8 assays (17). In this study, our videomicroscopy captured *pilT* mutant-infected cells undergoing apoptosis, and cell-sorting studies quantitated the number of apoptotic cells in wild-type (wt)- and *pilT* mutant-infected cultures. These data provide strong evidence that Tfp retraction plays an intrinsic cytoprotective role for the host during infection.

MATERIALS AND METHODS

Cell lines and bacterial strains. The A431 human epidermoid carcinoma cell line (obtained from S. Schmid) was used for these studies. The cells were maintained in Dulbecco's modified Eagle's medium (Mediatech) with 10% heat-inactivated fetal bovine serum (FBS) (Gibco) and incubated at 37°C and 5% CO_2. The bacterial strains used for these studies are derivatives of *N. gonorrhoeae* strain MS11, which expresses Tfp but not Opa (48). MS11*pilT* has a null mutation in *pilT*. It produces nonretractable Tfp and is nonmotile (38, 60). In MS11*pilT*i, the *pilT* open reading frame is under the control of the *lacZ* promoter. Isopropyl-β-D-thiogalactopyranoside (IPTG)-induced bacteria are motile (60) and form wt microcolonies (D. L. Higashi and M. So, unpublished observations). Bacteria were grown on GCB agar (Difco) with Kellog's supplements I and II and incubated at 37°C and 5% CO_2. The PilT expression, piliation, and Opa status of all strains were monitored by microscopic observation of colony morphology and immunoblotting with polyclonal antibodies against PilT (a gift of K. T. Forest) and monoclonal antibodies against pilin (36) and Opa (1).

Infections, transfections, and treatments. A431 cells were grown to 95% confluence in 35-mm glass bottom culture dishes (MaTek), on 6-well or 24-well microtiter plates (Falcon), or on coverslips. For actin-green fluorescent protein (GFP) studies, A431 cells were grown to 50% confluence in 35-mm dishes (Matek) and transfected with a pEGFP-Actin vector (Clontech), which encodes human cytoplasmic β-actin fused to the enhanced-GFP sequence, using Fugene 6 Transfection Reagent (Roche). At 48 h posttransfection, the cultures were used for infection or staurosporine (STS) (Sigma) treatment. For all infections, bacteria were harvested after 14 to 16 h of growth on agar plates, suspended in preequilibrated (37°C; 5% CO_2) tissue culture media, and added to the cells at a multiplicity of infection of 20 for 5.5 h unless otherwise indicated. For mock infections, preequilibrated tissue culture medium was added to uninfected cells at the start of the infection. For STS treatments, uninfected cells were incubated in STS (1 μM) in preequilibrated (37°C; 5% CO_2) tissue culture media for 4.5 h.

Live-cell microscopy. Live-cell imaging was done using a DVRT system (Applied Precision) with a Linux workstation and accompanying RedHat software in time-lapse mode. The system consists of an Olympus 1X-71 microscope base, a high-precision XYZ stage on an antivibration table, and an environmental chamber digitally controlled for heat and adapted for 5% CO_2 perfusion. The microscope is fitted with a 60× oil 1.4-numerical-aperture lens and a Nikon CoolSnap EM charge-coupled device camera.

For differential interference contrast (DIC) tracking experiments, A431 cells were grown to 95% confluence in 35-mm (Matek) dishes and mock infected with medium or infected with MS11 or MS11*pilT* for 5.5 h. DIC images were acquired every 2 min for 5.5 h.

For actin-GFP experiments, A431 cells expressing actin-GFP were grown in 35-mm dishes and infected with MS11 or MS11*pilT* for 5.5 h. After 30 min, DIC and fluorescein isothiocyanate (FITC) z stacks were acquired every 2.5 min for 5 h. Each z stack consisted of seven 1-μm-thick optical sections representing an area from the basolateral to the apical surface of the cells. For STS-treated uninfected cells, the images were acquired for 30 min prior to the addition of STS (1 μM), and imaging continued for an additional 4.5 h.

All images were processed at a Delta Vision Imaging Workstation with accompanying software. A single z-step DIC image was taken from each time point and constructed into a video using softWoRx. Projections of FITC images at each time point (seven z steps) were assembled into a video using softWoRx. All other video manipulations were done using QuickTime Pro (Apple) and Final Cut Express HD (Apple).

For each frame in the time-lapse image sequence of wt MS11 infection, the three uppermost z steps (apical region) were projected using softWoRx software. The DIC image and its corresponding FITC image were exported to Adobe Photoshop (version 7.0) and Adobe Illustrator (version 10.0) for manuscript preparation.

Tracking analysis. DIC images from the MS11 and MS11*pilT* infection videos were imported into Imaris (Bitplane). Microcolony tracking was performed using the Imaris tracking feature, which identifies the x and y coordinates for each microcolony at each time point. Trajectory plots of microcolony movements were generated, and statistics were exported to an Excel spreadsheet for further analysis. The plots and Excel graphs were exported to Adobe Photoshop (version 7.0) and Adobe Illustrator (version 10.0) for manuscript preparation.

Immunofluorescence microscopy. A431 cells were grown to 70 to 80% confluence on cover slips and mock infected with preequilibrated tissue culture medium, infected with MS11 or MS11*pilT* for 5.5 h, or incubated with STS for 4.5 h. The coverslips were then washed three times with phosphate-buffered saline (PBS), fixed in paraformaldehyde (4% [wt/vol] in PBS) for 20 min at room temperature, and blocked in blocking buffer-isotonic PBS containing normal goat serum (3% [vol/vol]; Gibco) and saponin (0.03% [wt/vol]; Sigma) for 1 h. To determine poly(ADP) ribose (PAR) levels, monoclonal antibody 10H (Alexis Biochemicals) was diluted in blocking buffer, added to samples, and incubated overnight in a moist chamber at 4°C. The coverslips were rinsed in PBS and incubated with Alexa-conjugated secondary antibody (Molecular Probes) diluted in blocking buffer for 1 h at 25°C. The samples were also subsequently incubated with the DNA stain DAPI (4′,6′-diamidino-2-phenylindole; diluted 1:1,000 in PBS) for 10 min to visualize nuclei. The samples were rinsed extensively with PBS before being mounted in Fluoromount-G (Southern Biotech). Negative control samples were processed as described above in the absence of primary antibody. Images were acquired on a Nikon Microphot-FX. DAPI and FITC channel images were merged using Magnafire software (Storz Imaging). The images were subsequently exported to Adobe Photoshop (version 7.0) and Adobe Illustrator (version 10.0) for manuscript preparation.

LDH assay. Lactate dehydrogenase (LDH) levels were determined using a colorimetric assay (Roche) as described previously (26). A431 cells were grown to 70 to 80% confluence in 24-well microtiter plates (Falcon) as described above. The cells were washed three times in assay medium consisting of phenol red-free Dulbecco's modified Eagle's medium (Mediatech) supplemented with 2.5% FBS and were incubated overnight in the same medium prior to the start of the experiment. A431 cells were mock infected with medium or infected with MS11 or MS11*pilT* for 5.5 h. Parallel sets of uninfected cells were treated with STS for 4.5 h or with Triton X-100 (Sigma) (1% [vol/vol] in medium) for 15 min. Culture supernatants were collected, centrifuged, and prepared according to the manufacturer's instructions, and the absorbance at an optical density of 490 nm was determined. For each sample, triplicate determinations were made and subtracted from those of the background controls. Values were normalized to uninfected controls and averaged, and the mean ± standard deviation (SD) was calculated. Statistical analysis was performed using the standard Student's t test.

Trypan blue exclusion assay. The trypan blue assay was performed as described previously (9). Briefly, A431 cells were grown to 95% confluence in 24-well plates and mock infected with medium or infected with MS11 or MS11*pilT* for 5.5 h. The cells were washed three times with PBS, collected, and stained with trypan blue (Gibco). Six fields of cells were counted (single blind) for the presence or absence of trypan blue stain. The percentage of viable cells in the culture was determined by the following formula and normalized to uninfected controls: (number of trypan blue-negative cells/total number of cells) × 100.

Flow cytometry assay. A431 cells were grown in six-well plates to 95% confluence and mock infected with medium or infected with MS11 or MS11*pilT* for 5.5 h or treated with STS for 4.5 h. For *pilT* induction experiments, A431 cells were mock infected with medium, with or without IPTG (2 mM), or infected with MS11*pilT*i in the presence or absence of IPTG (2 mM) for 5.5 h. (The induced MS11*pilT*i inoculum was harvested from agar plates containing 2 mM IPTG.) The cultures were washed three times with PBS, trypsinized, and collected in cold PBS containing 10% FBS. Suspensions were pelleted and resuspended in cold PBS. Samples were stained with propidium iodide (PI) and YO-PRO-1 (Vybrant Apoptosis Assay; Molecular Probes) according to the manufacturer's directions.

Green (FL-1) and red (FL-2) fluorescences were determined using a BD FACS Calibur flow cytometer (BD Biosciences) with a 488-nm Argon laser. Gating parameters were established using the forward and side scatter properties of uninfected, unlabeled cells. For all samples, 10,000 events within each gate were determined. The data were exported to FlowJo software (Ashland, OR) for analyses and plot generation.

Electron microscopy. A431 cells were grown to 95% confluence in 35-mm dishes and mock infected with medium or infected with MS11 or MS11*pilT* at a multiplicity of infection of 20 for 3 h. The cells were washed three times in PBS and fixed in PBS containing glutaraldehyde (2.5% [wt/vol]) overnight at 4°C. Samples were prepared as described previously (43). Briefly, cultures were washed three times in PBS and incubated in 1% osmium tetraoxide (1% in PBS

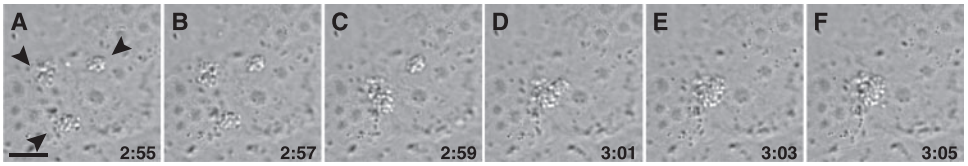

FIG. 1. Microcolony fusion and realignment. Time-lapse images of three fusing microcolonies (see Video S1 in the supplemental material) of A431 cells infected with wt MS11. The time stamps on the lower right corners indicate h:min postinfection. (A and B) Three microcolonies (arrowheads) before fusion. (C, D, E, and F) The same microcolonies undergoing fusion and realignment. Scale bar, 10 μm.

[wt/vol]; Electron Microscopy Sciences) for 1 h at room temperature. Samples were washed three times with PBS and dehydrated by successive incubations in ethanol (25%, 50%, 75%, and 95% [vol/vol] in water and 100%). The samples were treated with hexamethyldisilazane (Electron Microscopy Sciences) for 10 min and air dried in a laminar flow hood overnight. For imaging, samples were sputter coated with palladium and imaged on an FEI Siron Scanning Electron Microscope in the ultrahigh resolution mode.

RESULTS

PilT-dependent microcolony formation and microvillus deformation by *N. gonorrhoeae* during attachment. We used live-cell microscopy to determine the kinetics of *pilT*-mediated attachment. A431 human epithelial cells were infected with the wt *N. gonorrhoeae* strain MS11 or the retraction-deficient mutant MS11*pilT* or mock infected with medium. A431 is an established epidermoid carcinoma cell line that has been shown to support *Neisseria* attachment. Unless stated otherwise, all infections were performed for 5.5 h. Uninfected cells remained healthy throughout image acquisition (see Video S1, left panel, in the supplemental material). In cultures infected with wt bacteria, microcolonies formed continuously and were visible within 1 hour postinfection. Unexpectedly, microcolonies were also motile, and they fused to form larger motile structures. Microcolony motility and fusion were observed as late as 22 h postinfection (data not shown). Fusing microcolonies initially had a multilobed appearance, but they quickly reorganized into a smooth-edged spherical shape (see Video S1, middle panel, in the supplemental material) (Fig. 1). The re-sorting diplococci within these microcolonies suggest a level of bacterium-bacterium communication during fusion. Some microcolonies grew larger, apparently without fusing with other microcolonies. This size increase could be due to bacterial division or fusion with bacteria not readily visible by microscopy, or both.

The distinctive domed shape of wt microcolonies and the bilobed shape of two fusing microcolonies were further illustrated by scanning electron microscopy (SEM) of MS11-infected monolayers (Fig. 2B and C, respectively). Microcolonies were observed to localize on the host cell surface, as well as in the junctions between cells. These images also reveal the close association of microvilli with bacteria and the elongated appearance of these microvilli at the microcolony periphery. Previous microscopy of *Neisseria*-infected tissue segments revealed similar microvillus rearrangments beneath microcolonies (30, 52, 53). Our study additionally demonstrates the ability of an individual bacterium to induce these changes in the host cell microvilli (Fig. 2B).

In constrast to wt MS11, the retraction-deficient MS11*pilT* formed nonmotile, irregularly shaped clusters that were clearly observed by live-cell microscopy (see Video S1, right panel, in the supplemental material) and SEM (Fig. 2D). Elongated microvilli were rarely seen in MS11*pilT*-infected cells (Fig. 2D), in contrast to MS11-infected cells (Fig. 2B and C), suggesting that Tfp retraction triggers the alteration of microvillus architecture.

Trajectory of microcolony movement. We next analyzed the videomicroscopy data to determine how far microcolonies traveled over time (displacement) and whether their movements were vectorial (directional). The movements of wt and *pilT* microcolonies on epithelial cells were recorded over a 5.5-hour period (see Materials and Methods). The position of each microcolony was analyzed by compiling successive frames of the movie into a "trajectory map" to illustrate the path taken by the microcolony along the *xy* axes (Fig. 3A). A displacement graph was also generated to determine the distance traveled by each microcolony from its point of origin as a function of time (Fig. 3B). The results show that wt microcolonies migrated greater distances from their point of origin than *pilT* microcolonies (22.2 ± 12 μm and 6.4 ± 2.6 μm, respectively). However, the trajectory data do not allow us to draw any conclusions about the directionality of movement.

Together, these studies show that Tfp-mediated attachment to epithelial cells is a multidimensional process that involves continuous interactions among bacteria, as well as between the bacteria and their host.

PilT-dependent cortical plaque formation and maintenance. Immunofluorescence microscopy studies showed that Tfp retraction induces the formation of cortical plaques in the infected cell 3 h postinfection. These plaques contain high concentrations of a number of host components, including actin (36). The dynamic nature of microcolony formation and motility led us to follow cortical plaque formation in real time during attachment. A431 cells expressing actin-GFP were infected with wt MS11 or MS11*pilT*. Fluorescence (FITC) and DIC images of infected cells were acquired every 2.5 min for 5 h beginning 30 min postinfection and assembled into videos (see Videos S2 and S3 in the supplemental material).

Images from the wt MS11 video (see Video S2 in the supplemental material) were assembled into panels to illustrate key events of infection (Fig. 4A and B). The corresponding FITC and DIC images were compared to locate actin-GFP plaques relative to the position of the microcolony. An actin plaque was observed upon entry of a microcolony onto the epithelial cell (Fig. 4A, ii to iv; see Video S2 in the supplemental material). At the fullest extent of plaque formation, actin accumulation was particularly dense at the periphery of the structure (Fig. 4A and B). This concentration of actin at the microcolony edge was also observed in fixed cell preparations (data not shown). Actin plaques comigrated with motile

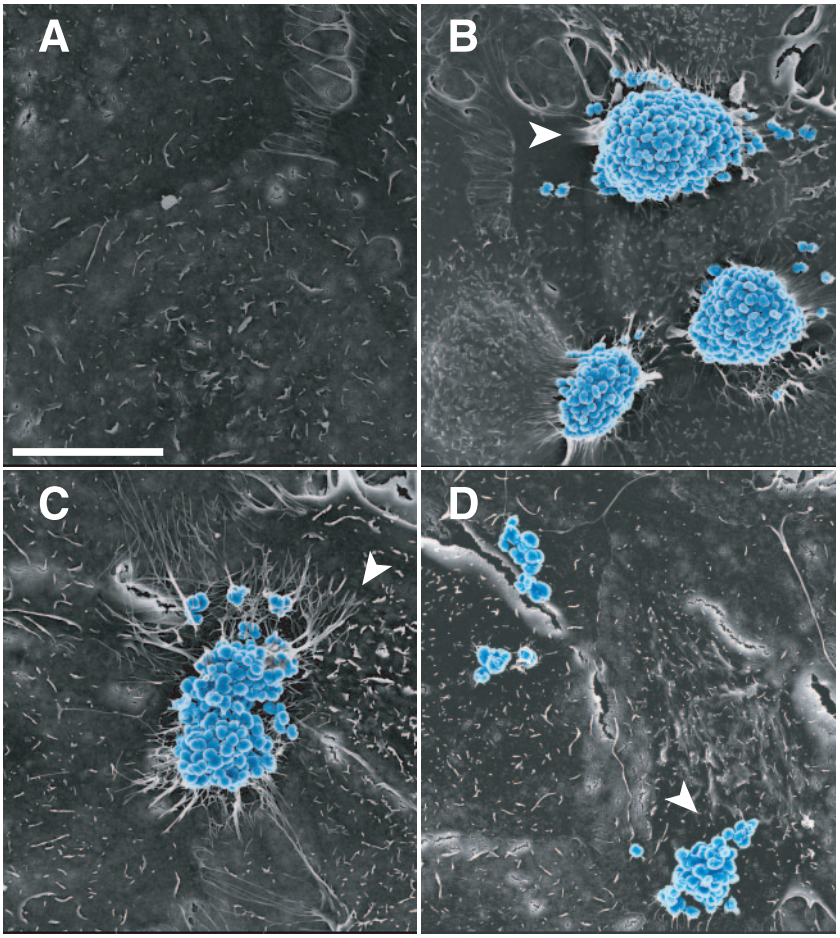

FIG. 2. Shapes of wt and *pilT* mutant microcolonies and morphologies of host cell microvilli. Shown are SEM images of A431 cells incubated for 3 h with medium (A), wt MS11 (B and C), or MS11*pilT* (D). Bacteria are color enhanced (blue) to provide added contrast with the epithelial cells (gray). (B and C) Domed and bilobed shapes of wt microcolonies. The arrowheads point to stretched and elongated microvilli beneath microcolonies. Other microvilli appear to wrap around individual diplococci at the peripheries of, or away from, microcolonies. (A) Morphology of the mock-infected cell surface. (D) Irregular shape of MS11*pilT* clusters and lack of microvillus remodeling. Scale bar, 10 μm.

microcolonies (Fig. 4A and B). In contrast, MS11*pilT* did not trigger actin plaque formation (see Video S3 in the supplemental material), although the mutant adhered to epithelial cells as well as wt MS11 (33) and formed aggregates on the cell surface. These observations strongly suggest that the presence of the microcolony, as well as retractile force from the microcolony, are necessary for actin plaque formation and maintenance. (The DIC images in Fig. 4B also show the fusion of two microcolonies and the rapid [within 6 min, as shown in images ii to iv] reorganization of its shape.)

These results demonstrate the highly kinetic nature of the cortical plaque and reinforce our previous finding that plaque formation requires Tfp retraction (33). Importantly, they demonstrate that actin plaque formation and maintenance require continuous microcolony stimulation through Tfp retraction. Similar responses were also observed with ezrin, a member of the ezrin/radixin/moesin family of cytoskeletal linkers that is also a cortical plaque component (data not shown).

Cytotoxicity induced by the *pilT* mutant MS11*pilT*. Cell death was repeatedly observed in MS11*pilT*-infected cultures, but not in MS11-infected cultures (see Videos S3 and S2, respectively, in the supplemental material). Dying cells were characterized by cell condensation, bleb formation, and ultimately membrane-bound cellular fragmentation (Fig. 5A). To examine the nature of these dying cells, trypan blue cell viability assays were performed (9). Twenty-two percent (±16% SD) of the cells infected with MS11*pilT* for 5.5 h excluded trypan blue compared to uninfected control cells. In contrast, 78% (±18% SD) of MS11-infected cultures excluded the dye. The difference in cytotoxicity between wt and *pilT* is unlikely to be due to a variation in bacterial growth, as both strains grew equally well in liquid media and on tissue culture cells (data not shown).

Apoptotic cell death in MS11*pilT*-infected cultures. Eucaryotic cell death is traditionally defined by the morphological changes associated with the dying cell (20). Apoptosis is characterized by the condensation of the nucleus and cytoplasm, followed by membrane-bound fragmentation of the cell. Necrosis is typified by organelle and cellular swelling, followed by a rupture of the plasma membrane (19). We next imaged STS-induced cell death (4) to compare it to the morphological features of dying cells in *pilT*-infected cultures. STS is a cell-

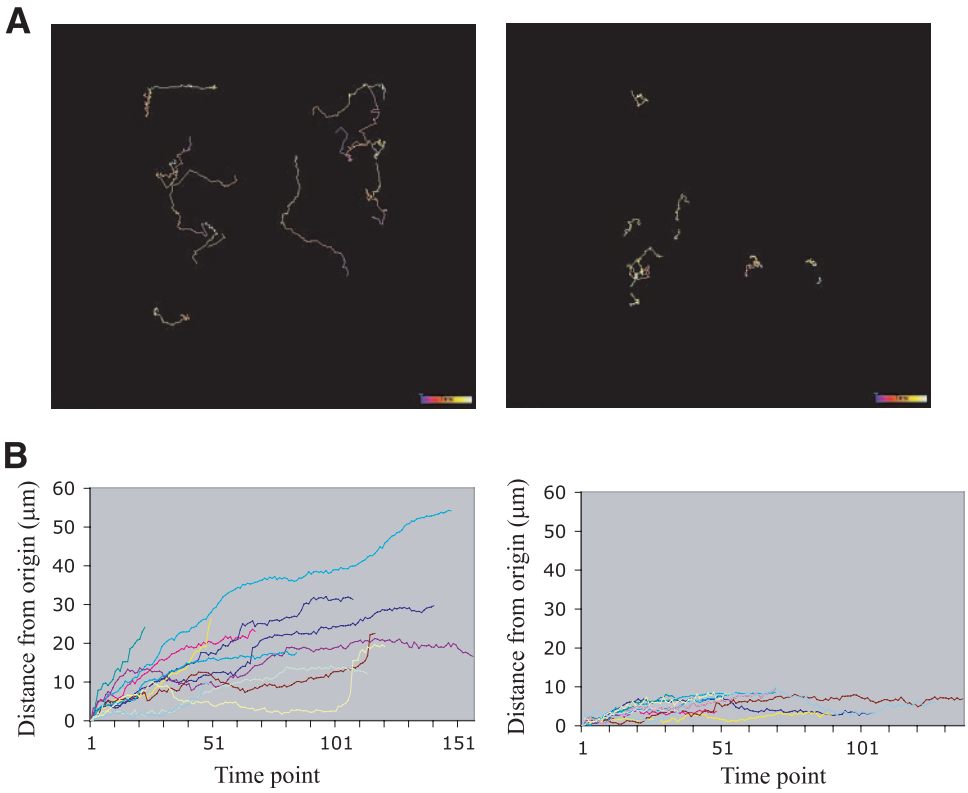

FIG. 3. Movement of wt and *pilT* microcolonies during infection. (A) Trajectories of the movements of wt MS11 (left) and MS11*pilT* (right) microcolonies on A431 epithelial cells over a 5.5-hour infection (see Materials and Methods for details). The color code in each track shows the time of image acquisition. Blue represents the beginning of image acquisition. White represents the end of image acquisition. Color bar, 5.5 h. (B) Distances traveled by microcolonies from the point of origin expressed as a function of time (each unit represents 2 min) for wt MS11 (left) and MS11*pilT* (right).

permeable protein kinase inhibitor that is used to induce apoptosis in a variety of cell lines. Actin-GFP-expressing A431 cells were imaged for 30 min. STS (1 μM) was added, and the cells were imaged for an additional 4.5 h. Upon addition of STS, there was an immediate cessation of actin activity, followed by cell condensation and fragmentation into apoptotic bodies (see Video S4 in the supplemental material). A series of images from the video is shown in Fig. 5B. These studies reveal that *pilT*- and STS-induced cell death display very similar morphological features (Fig. 5A and B).

Previously, we reported that *pilT*-infected T84 human epithelial cells had higher levels of cleaved PARP and cleaved caspase 8 than wt-infected or uninfected cells (17). Here, we assessed apoptosis in MS11- and MS11*pilT*-infected A431 cells for their levels of PAR polymer. As a downstream product of activated PARP, PAR is a more direct readout of apoptosis (10, 21). A431 cells were infected with MS11 or MS11*pilT* or mock infected in the presence or absence of STS. Consistent with our previous findings, PAR was clearly visible in many cells infected with MS11*pilT* or treated with STS. It was barely visible or absent in uninfected or MS11-infected cells (Fig. 6). Taken together, these results indicate that infection with a *pilT* mutant triggers apoptotic cell death.

Flow cytometry analysis of MS11*pilT*-associated apoptosis. We next used flow cytometry to examine the cytotoxicity observed in MS11*pilT*-infected cultures. A431 cells were infected with wt MS11 or MS11*pilT* or mock infected. Parallel uninfected cultures were treated with STS as a positive control for apoptosis (5, 22). The cells were stained with YO-PRO-1 and PI and analyzed by flow cytometry (18). YO-PRO-1 uptake corresponds to an increase in membrane permeability, an early indicator of apoptosis, while PI staining indicates cell death. Gating for forward and side scatter properties was established with a healthy population of uninfected, unlabeled cells (see Materials and Methods). Bivariate dot plots of PI and YO-PRO-1 fluorescence were generated (Fig. 7A, top) using the gated populations shown in their respective scattergrams (Fig. 7A, bottom). Early apoptosis was measured by the uptake of YO-PRO-1, while late apoptosis and cell death were measured by the uptake of both YO-PRO-1 and PI (42, 55). To express the levels of cell death, viability was scored on the basis of the uptake of both dyes (YO-PRO-1$^+$ PI$^+$), as shown in elliptical region D of the upper images.

Mock-infected cultures had few nonviable cells (2.32% YO-PRO-1$^+$ PI$^+$; 0.03% YO-PRO-1$^+$ PI$^-$). In MS11-infected cultures, 6.16% of cells were YO-PRO-1$^+$ PI$^+$ and 0.25% were YO-PRO-1$^+$ PI$^-$, indicating that wt *N. gonorrhoeae* had a very small effect on viability. In contrast, 69.9% of cells in MS11*pilT*-infected cultures were YO-PRO-1$^+$ PI$^+$ and 0.04% were YO-PRO-1$^+$ PI$^-$. Thus, the *pilT* mutant substantially decreased host cell viability. These results are consistent with the trypan blue observations. The low proportion (1.08%) of

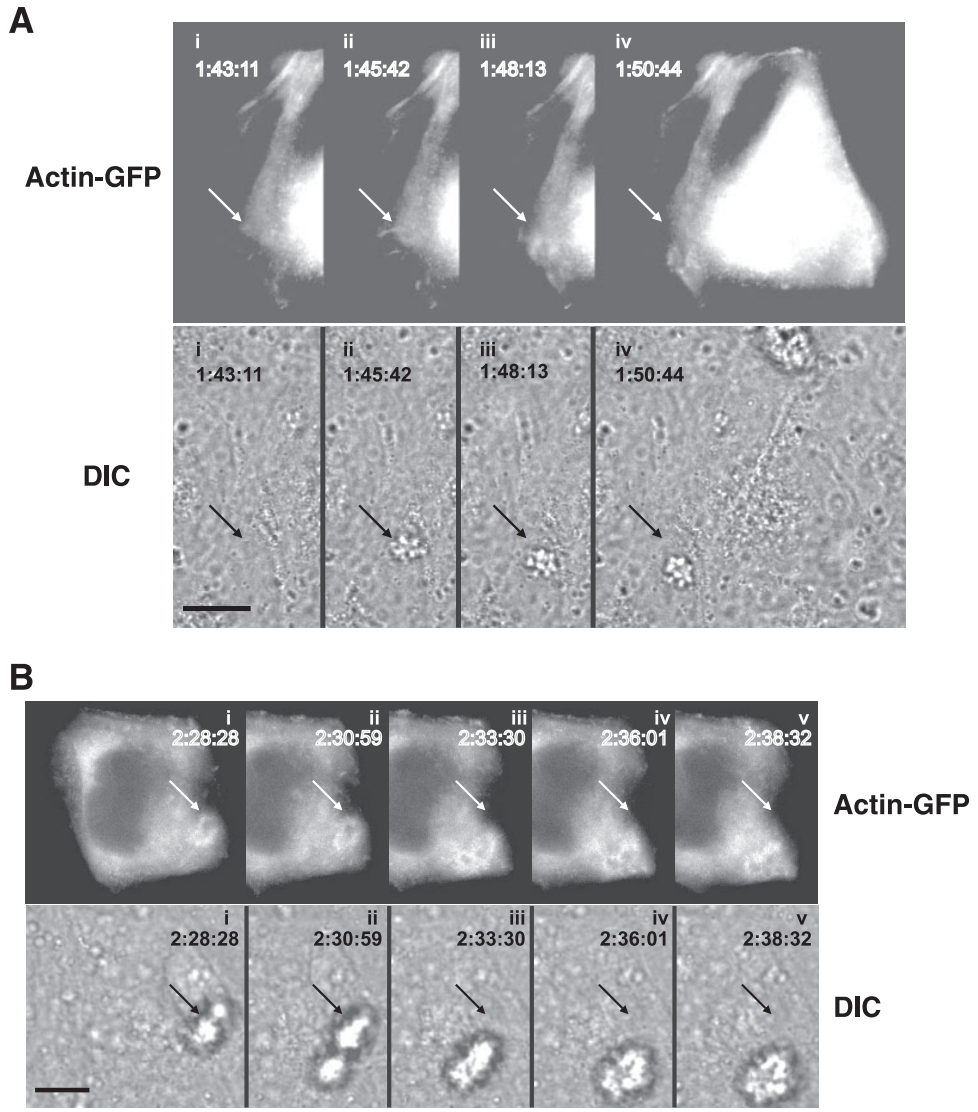

FIG. 4. Positions of actin-GFP plaques relative to a moving microcolony. Time-lapse images (see Video S2 in the supplemental material) were compiled to show two different actin-GFP-expressing A431 epithelial cells with infecting wt MS11 microcolonies. The time stamps indicate the times of image acquisition in hr:min:s. (A) Clustering of actin-GFP at the site of entry of a microcolony. (Top) Successive FITC images showing actin-GFP clustering in the cell. Directly below each FITC image is the corresponding DIC image, presented to show the position of the microcolony. Frame i was acquired prior to entry of the microcolony onto the cell. The arrow points to the entry site of the microcolony; its position in all frames is invariant. (B) Movement of actin-GFP plaque relative to the position of a motile microcolony. (Top) Successive FITC images of another infected cell showing the positions of the actin-GFP plaque. Directly below each FITC image is the corresponding DIC image showing the positions of the microcolony. The arrow in each panel points to the original position of the microcolony; its position in all frames is invariant. Scale bar, 10 μm.

YO-PRO-1$^+$ PI$^+$ cells in the STS-treated culture is due to the fact that many of the cells within the gated population were still in the very early stages of apoptosis and therefore stained only with YO-PRO-1 (upper right image, triangular region A).

We verified the role of *pilT* in cytotoxicity using an IPTG-inducible *pilT* strain. In MS11*placZ-pilT* (MS11*pilT*i), the *pilT* gene is under the control of the IPTG-inducible *lacZ* promoter (23, 60). On epithelial monolayers in the presence of IPTG, MS11*pilT*i forms microcolonies with wt morphology and triggers cortical plaque formation (data not shown). A431 cells were infected with MS11*pilT*i in the presence or absence of IPTG. Parallel cultures were mock infected with medium in the presence or absence of IPTG. After 5.5 h, the cultures were processed for flow cytometry and scored for cell viability as described above. Uninfected cultures with or without IPTG had similarly low levels of YO-PRO-1$^+$ PI$^+$ and YO-PRO-1$^+$ PI$^-$ cells (Fig. 7B). In cultures infected with MS11*pilT*i without IPTG, 64.2% of cells were YO-PRO-1$^+$ PI$^+$. This percentage dropped to 36% when cultures were infected with MS11*pilT*i in the presence of IPTG. Thus, inducing *pilT* expression during infection partially, but significantly, reverses the cytotoxicity caused by the *pilT* mutant. Together, these results demonstrate that a functional *pilT* is important for maintaining host cell viability.

Quantitating LDH release in MS11*pilT*-infected cells. Finally, we determined whether necrosis played a role in the

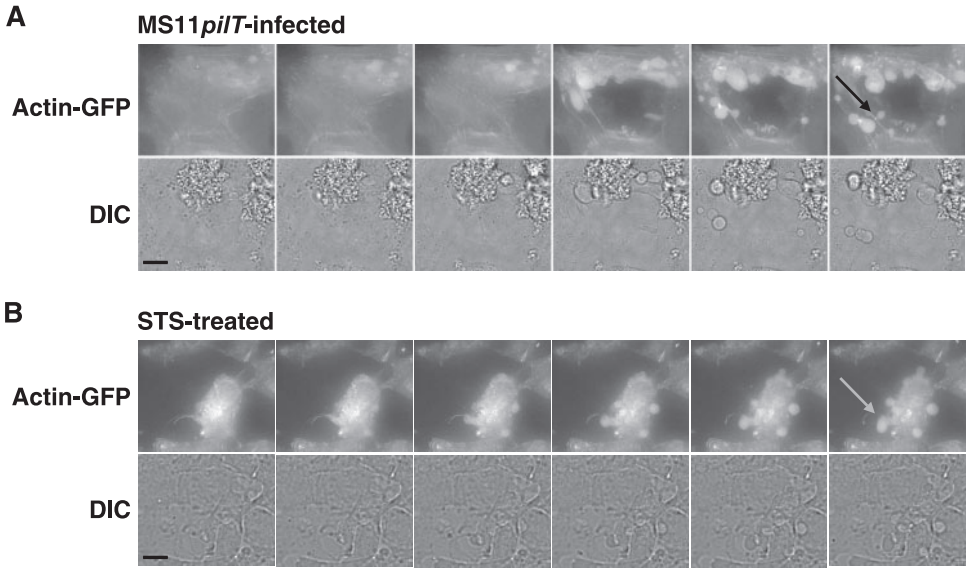

FIG. 5. Morphology of actin-GFP-expressing A431 cells infected with MS11*pilT* (A) or treated with the apoptosis-inducing agent STS (B). The images in panels A and B are taken from successive video images (see Videos S3 and S4, respectively, in the supplemental material). The top rows in panels A and B show FITC images of A431 cells. The DIC image corresponding to each FITC image appears immediately below. Both sets of images were acquired over a 12.5-min period. The arrows indicate apoptotic bodies. Scale bar, 11 μm.

cytotoxicity observed in *pilT*-infected cultures. Necrotic cell death is accompanied by membrane damage and the release of cytoplasmic components, such as LDH, into the medium (19, 41). In contrast, apoptotic cells suffer little membrane damage and cytoplasmic contents remain within the dying cell. We therefore measured the LDH activities of cell supernatants (26) to assess necrosis. A431 cells were infected with wt MS11 or MS11*pilT* or mock infected. As positive and negative controls, mock-infected cultures were treated with Triton X-100 or STS, respectively. Cell-free supernatants were assayed for LDH activity. Relative to uninfected cells (with their LDH activities arbitrarily set at 1.0), Triton-treated cells released substantial amounts of LDH (114.98 ± 4.92), while STS-treated cells did not (1.33 ± 0.80). Importantly, MS11*pilT*-infected cells released little LDH relative to uninfected cells (0.67 ± 0.29). Thus, cell death resulting from *pilT* infection does not involve membrane damage. MS11-infected cells released the smallest amount of LDH of all the samples (0.26 ± 0.15). In fact, they released significantly less LDH than uninfected cells ($P < 0.005$), indicating that membranes of wt-infected cells are healthy.

DISCUSSION

Studies of *N. gonorrhoeae*-host cell interactions have yielded inspiring information on this subject and identified hallmarks of Tfp-mediated attachment (30, 33, 52, 59). Bacteria were often observed to attach to epithelial cells as microcolonies and to cause dramatic changes in the infected cell cortex, elongating and deforming microvilli and recruiting host cell components to the site of attachment. Other studies have demonstrated the retractile nature of Tfp and the importance of retraction in twitching motility, intimate attachment to host cells, and induction of host cell responses (23, 38, 45). These attributes of Tfp raise important questions regarding the timing and kinetics of attachment. Where do these "snapshots" of infection, derived from fixed-cell studies, fit within this framework of bacterial motility and ensuing host responses? Our study showed that Tfp-mediated attachment is a dynamic process. Microcolony formation, motility, and fusion occur continuously. The host cell responds to this Tfp stimulation. Cortical plaques are observed to form, dissociate, and re-form under moving microcolonies. These events engage downstream

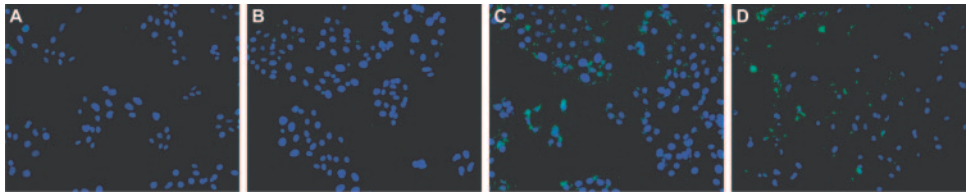

FIG. 6. Immunodetection of PAR in infected A431 cells. A431 cells were mock infected with medium (A), infected with wt MS11 (B) or MS11*pilT* (C) for 5.5 h, or treated with STS for 4.5 h (D). Samples were fixed and stained with antibodies to PAR (green) and DAPI (blue) to visualize nuclei. All images were acquired on a Nikon Microphot-FX at the same magnification. PAR and DAPI signals are superimposed in all images.

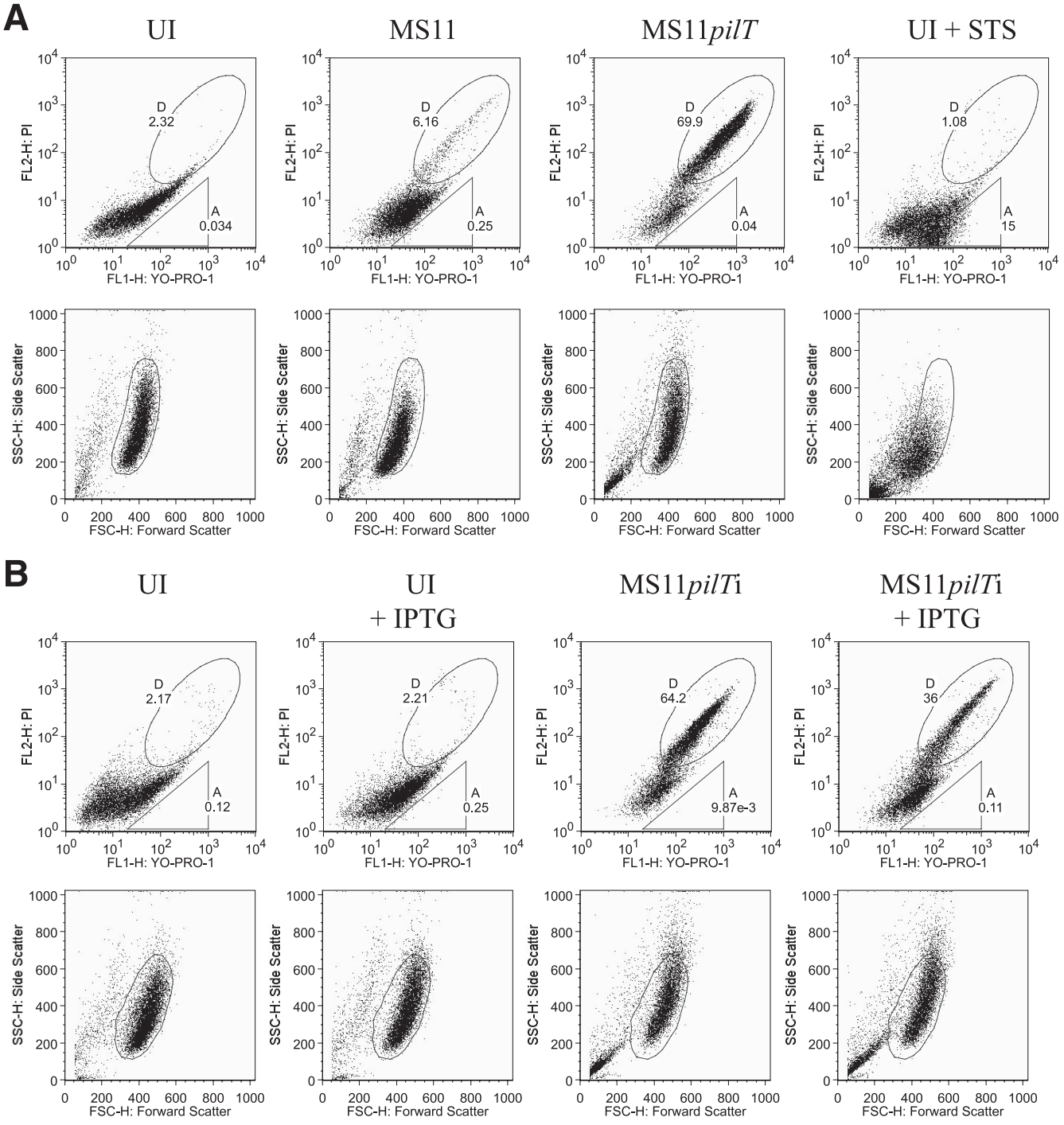

FIG. 7. Dual-fluorescence flow cytometry analysis of cell death in *N. gonorrhoeae*-infected cultures. (A) A431 cells were mock infected with medium (UI), infected with wt MS11 or MS11*pilT* for 5.5 h, or treated with STS for 4.5 h and analyzed by flow cytometry for YO-PRO-1 and PI staining (top row). (B) A431 cells were infected with MS11*pilT*i in the presence or absence of IPTG. Parallel mock-infected (UI) cultures were treated with IPTG or left untreated, as indicated (see Materials and Methods), and analyzed by flow cytometry for YO-PRO-1 and PI staining. The top rows in panels A and B contain bivariate dot plots of cells in each sample stained with these dyes. The number in gate A indicates the percentage of YO-PRO-1$^+$ PI$^-$ cells in the population. The number in gate D indicates the percentage of YO-PRO-1$^+$ PI$^+$ cells. Below each sample is its corresponding scattergram (lower rows). The gated populations within each scattergram were used to plot PI fluorescence in relation to YO-PRO-1.

host cell signaling cascades, one consequence of which is to confer cytoprotection on the host.

How does Tfp retraction lead to microcolony movement? Multiple Tfp are expressed on the *N. gonorrhoeae* surface, apparently in a nonpolar fashion. For twitching motility to take place, retraction is assumed to be coordinated. Our study did not address this issue at the molecular level; however, the ability of a microcolony to crawl indicates that Tfp retraction

occurs within the structure and that retraction is coordinated. In turn, coordinated Tfp retraction suggests that the bacteria within the microcolony communicate at some level. The idea of bacterial communication and coordinated retraction is further supported by the observation that newly fused microcolonies rapidly change their shapes. Bacterial realignment occurs only in wt microcolonies and not in *pilT* mutant aggregates. Similarly, the intricate Tfp-based movements of *C. perfringens* and *X. fastidiosa* on agar surfaces also imply communication and coordination (32, 56).

Microcolonies fused into larger motile structures over a period of 5 h and up to 22 h, when the experiment was terminated. This implies that epithelial cells could experience increasingly higher tensile forces over time as microcolonies develop into larger structures that are capable of "pulling" with greater force. Indeed, retraction forces of 1 nN were recently recorded from *N. gonorrhoeae* microcolonies (N. Biais, unpublished data). Epithelial cells responded to Tfp retraction forces as early as 15 min postinfection (17, 23). It remains to be determined whether and how dynamic changes in the level of force exerted over the course of infection might stimulate the host.

Previous fixed-cell studies showed that Tfp retraction induces the formation of cortical plaques beneath attached *N. gonorrhoeae* microcolonies. Here, we revealed the kinetic nature of plaque development and showed that plaque maintenance requires continuous microcolony stimulation through Tfp retraction. The speed of these actin rearrangements is consistent with the rapid rate of actin assembly and disassembly (6, 44, 51). The mechanism(s) of actin plaque formation is unknown but could involve phosphatidylinositol 3-kinase and/or mitogen-activated protein kinases. These stress-responsive signal cascades participate in cytoskeleton remodeling and are activated by Tfp retraction (17, 23).

N. gonorrhoeae infection promotes the quiescence of host cells during the early stages of infection (7, 39, 49). The *N. meningitidis* porin has been shown to exert a cytoprotective effect (27, 28). Tfp retraction in *N. gonorrhoeae* also lowers apoptosis signaling, either directly or indirectly, as judged by cleaved-PARP and caspase 8 assays (17). Here, we provide visual evidence of *pilT*-infected, actin-GFP-expressing cells undergoing apoptosis. While it is formally possible that the stress of transfection and/or expression of the actin-GFP construct may have sensitized cells to apoptosis, we believe this to be an unlikely contributor to the *pilT* cytotoxicity, as the actin-GFP-expressing cells infected with wt bacteria were healthy. Furthermore, the relative cytotoxicity of the *pilT* mutant was also observed in subsequent experiments using nontransfected cells. We also provide quantitative evidence that *pilT*-infected cultures have significantly more apoptotic cells than wt-infected cultures and that IPTG induction of *pilT* in the MS11*pilT*i mutant partially overcomes this cytotoxicity. These results provide strong additional support for the role of Tfp retraction in promoting cytoprotection. Our study does not address the role of porin in this process, nor is it designed to determine whether retraction facilitates the presentation of porin to the host cell membrane. It is unclear why IPTG induction of *pilT* did not fully reverse the cytotoxicity of the MS11*pilT*i mutant. Induction may not have restored *pilT* expression or PilT function to wt levels. Alternatively, a component unrelated to PilT may also affect Tfp retraction or cytotoxicity.

The growth of adherent wt *N. meningitidis* was recently observed by videomicroscopy (25). This study showed that *N. meningitidis* forms microcolonies and large aggregates during attachment and growth on endothelial cells under shear stress conditions. It did not explore the contribution of Tfp-retraction (*pilT*) to these processes. Utilizing electron microscopy, another study determined that wt and *pilT* mutant *N. meningitidis* bacteria attach to epithelial cells in phenotypically similar manners early in infection (45). Both studies concluded that *pilT* does not contribute to the early stages of *N. meningitidis* attachment. In contrast, our study demonstrates the importance of *pilT* in *N. gonorrhoeae* microcolony development, host microvillus and cortical actin remodeling, and cytoprotection. Further studies will be needed to determine whether these disparate results regarding *pilT* reflect a basic difference in the attachment behaviors of *N. gonorrhoeae* and *N. meningitidis*.

What might be the function(s) of motile *N. gonorrhoeae* microcolonies during an infection of the human body? The ability of bacterial communities to move and interact with one another may better equip them to deal with environmental pressures. In *N. gonorrhoeae* human challenge studies, inoculation is followed by an "eclipse" period of 40 h during which bacteria cannot be cultured and patients are asymptomatic (8, 11, 14, 47). It is possible that microcolony stimulation (via Tfp retraction) during the attachment phase makes epithelial cells less sensitive to toxic bacterial products and/or activates receptors that promote infection. Indeed, cytoprotection, receptor activation, and invasion functions of Tfp retraction have been demonstrated in cultured cells (17, 23). Retraction, microcolony formation, and the host response may represent components in a positive-feedback loop that promote infection while maintaining host cell viability.

Microbial motility and aggregation have been observed in an ever-growing number of pathogenic organisms, from *Proteobacteria* and *Firmicutes* to protozoans, such as *Plasmodium falciparum* and *Trypanosoma brucei* (16, 57). Studies have uncovered important features of microbial behavior and pathogenesis, such as intraspecies dynamics and cell-to-cell spread. Importantly, they illustrate a recurring theme: organisms use cooperative motility to exploit their respective niches. To our knowledge, our study is the first to reveal the dynamics of host cell attachment and the importance of Tfp retraction to this process. As other bacterial pathogens also express retractile Tfp, our studies may have important implications for a general role of Tfp in virulence.

ACKNOWLEDGMENTS

We thank Colleen Witt for her critical comments on the tracking studies and Yoshinobu Koguchi, Mandy Boyd, Chunfei Li, and Ashlee Moses for expert assistance with microscopy and flow cytometry studies. We also thank Caroline Enns, Nicolas Biais, and members of the So laboratory for helpful comments on the manuscript and Chris Langford and Jeff Vandehey for their help in manuscript preparation. Finally, we also thank Katrina T. Forest for her kind gift of PilT antibodies.

This work was funded by NIH grants AI049973 and AI068033 awarded to M. So.

REFERENCES

1. **Achtman, M., M. Neibert, B. A. Crowe, W. Strittmatter, B. Kusecek, E. Weyse, M. J. Walsh, B. Slawig, G. Morelli, A. Moll, et al.** 1988. Purification and characterization of eight class 5 outer membrane protein variants from a clone of *Neisseria meningitidis* serogroup A. J. Exp. Med. **168:**507–525.
2. **Aukema, K. G., E. M. Kron, T. J. Herdendorf, and K. T. Forest.** 2005. Functional dissection of a conserved motif within the pilus retraction protein PilT. J. Bacteriol. **187:**611–618.
3. **Ayala, P., J. S. Wilbur, L. M. Wetzler, J. A. Tainer, A. Snyder, and M. So.** 2005. The pilus and porin of *Neisseria gonorrhoeae* cooperatively induce Ca^{2+} transients in infected epithelial cells. Cell. Microbiol. **7:**1736–1748.
4. **Belmokhtar, C. A., J. Hillion, and E. Segal-Bendirdjian.** 2001. Staurosporine induces apoptosis through both caspase-dependent and caspase-independent mechanisms. Oncogene **20:**3354–3362.
5. **Bernard, B., T. Fest, J. L. Pretet, and C. Mougin.** 2001. Staurosporine-induced apoptosis of HPV positive and negative human cervical cancer cells from different points in the cell cycle. Cell Death. Differ. **8:**234–244.
6. **Bershadsky, A. D., C. Ballestrem, L. Carramusa, Y. Zilberman, B. Gilquin, S. Khochbin, A. Y. Alexandrova, A. B. Verkhovsky, T. Shemesh, and M. M. Kozlov.** 2006. Assembly and mechanosensory function of focal adhesions: experiments and models. Eur. J. Cell Biol. **85:**165–173.
7. **Binnicker, M. J., R. D. Williams, and M. A. Apicella.** 2003. Infection of human urethral epithelium with *Neisseria gonorrhoeae* elicits an upregulation of host anti-apoptotic factors and protects cells from staurosporine-induced apoptosis. Cell. Microbiol. **5:**549–560.
8. **Cohen, M. S., J. G. Cannon, A. E. Jerse, L. M. Charniga, S. F. Isbey, and L. G. Whicker.** 1994. Human experimentation with *Neisseria gonorrhoeae*: rationale, methods, and implications for the biology of infection and vaccine development. J. Infect. Dis. **169:**532–537.
9. **Coligan, J. E.** 2005. Short protocols in immunology: a compendium of methods from current protocols in immunology. John Wiley & Sons, Hoboken, NJ.
10. **Donzelli, M., C. Negri, A. Mandarino, L. Rossi, E. Prosperi, I. Frouin, R. Bernardi, A. Burkle, and A. I. Scovassi.** 1997. Poly(ADP-ribose) synthesis: a useful parameter for identifying apoptotic cells. Histochem. J. **29:**831–837.
11. **Edwards, J. L., and M. A. Apicella.** 2004. The molecular mechanisms used by *Neisseria gonorrhoeae* to initiate infection differ between men and women. Clin. Microbiol. Rev. **17:**965–981.
12. **Felsenfeld, D. P., P. L. Schwartzberg, A. Venegas, R. Tse, and M. P. Sheetz.** 1999. Selective regulation of integrin—cytoskeleton interactions by the tyrosine kinase Src. Nat. Cell Biol. **1:**200–206.
13. **Forest, K. T., K. A. Satyshur, G. A. Worzalla, J. K. Hansen, and T. J. Herdendorf.** 2004. The pilus-retraction protein PilT: ultrastructure of the biological assembly. Acta Crystallogr. D. **60:**978–982.
14. **Handsfield, H., and P. Sparling.** 1995. Principles and practice of infectious diseases, 4th ed., vol. 2. Churchill Livingstone, New York, NY.
15. **Herdendorf, T. J., D. R. McCaslin, and K. T. Forest.** 2002. *Aquifex aeolicus* PilT, homologue of a surface motility protein, is a thermostable oligomeric NTPase. J. Bacteriol. **184:**6465–6471.
16. **Hill, K. L.** 2003. Biology and mechanism of trypanosome cell motility. Eukaryot. Cell **2:**200–208.
17. **Howie, H. L., M. Glogauer, and M. So.** 2005. The *N. gonorrhoeae* type IV pilus stimulates mechanosensitive pathways and cytoprotection through a *pilT*-dependent mechanism. PLoS Biol. **3:**627–637.
18. **Idziorek, T., J. Estaquier, F. De Bels, and J. C. Ameisen.** 1995. YOPRO-1 permits cytofluorometric analysis of programmed cell death (apoptosis) without interfering with cell viability. J. Immunol. Methods **185:**249–258.
19. **Kanduc, D., A. Mittelman, R. Serpico, E. Sinigaglia, A. A. Sinha, C. Natale, R. Santacroce, M. G. Di Corcia, A. Lucchese, L. Dini, P. Pani, S. Santacroce, S. Simone, R. Bucci, and E. Farber.** 2002. Cell death: apoptosis versus necrosis. Int. J. Oncol. **21:**165–170.
20. **Kerr, J. F., A. H. Wyllie, and A. R. Currie.** 1972. Apoptosis: a basic biological phenomenon with wide-ranging implications in tissue kinetics. Br. J. Cancer **26:**239–257.
21. **Koh, D. W., T. M. Dawson, and V. L. Dawson.** 2005. Mediation of cell death by poly(ADP-ribose) polymerase-1. Pharmacol. Res. **52:**5–14.
22. **Kopitar-Jerala, N., A. Schweiger, R. M. Myers, V. Turk, and B. Turk.** 2005. Sensitization of stefin B-deficient thymocytes towards staurosporin-induced apoptosis is independent of cysteine cathepsins. FEBS Lett. **579:**2149–2155.
23. **Lee, S. W., D. L. Higashi, A. Snyder, A. J. Merz, L. Potter, and M. So.** 2005. PilT is required for PI(3,4,5)P3-mediated crosstalk between *Neisseria gonorrhoeae* and epithelial cells. Cell. Microbiol. **7:**1271–1284.
24. **Maier, B., L. Potter, M. So, C. D. Long, H. S. Seifert, and M. P. Sheetz.** 2002. Single pilus motor forces exceed 100 pN. Proc. Natl. Acad. Sci. USA **99:**16012–16017.
25. **Mairey, E., A. Genovesio, E. Donnadieu, C. Bernard, F. Jaubert, E. Pinard, J. Seylaz, J. C. Olivo-Marin, X. Nassif, and G. Dumenil.** 2006. Cerebral microcirculation shear stress levels determine *Neisseria meningitidis* attachment sites along the blood-brain barrier. J. Exp. Med. **203:**1939–1950.
26. **Martin, A., and M. Clynes.** 1991. Acid phosphatase: endpoint for in vitro toxicity tests. In Vitro Cell Dev. Biol. **27A:**183–184.
27. **Massari, P., Y. Ho, and L. M. Wetzler.** 2000. *Neisseria meningitidis* porin PorB interacts with mitochondria and protects cells from apoptosis. Proc. Natl. Acad. Sci. USA **97:**9070–9075.
28. **Massari, P., C. A. King, A. Y. Ho, and L. M. Wetzler.** 2003. Neisserial PorB is translocated to the mitochondria of HeLa cells infected with *Neisseria meningitidis* and protects cells from apoptosis. Cell. Microbiol. **5:**99–109.
29. **Mattick, J. S.** 2002. Type IV pili and twitching motility. Annu. Rev. Microbiol. **56:**289–314.
30. **McGee, Z. A., A. P. Johnson, and D. Taylor-Robinson.** 1981. Pathogenic mechanisms of *Neisseria gonorrhoeae*: observations on damage to human fallopian tubes in organ culture by gonococci of colony type 1 or type 4. J. Infect. Dis. **143:**413–422.
31. **McGee, Z. A., D. S. Stephens, L. H. Hoffman, W. F. Schlech III, and R. G. Horn.** 1983. Mechanisms of mucosal invasion by pathogenic *Neisseria*. Rev. Infect. Dis. **4:**S708–S714.
32. **Meng, Y., Y. Li, C. D. Galvani, G. Hao, J. N. Turner, T. J. Burr, and H. C. Hoch.** 2005. Upstream migration of *Xylella fastidiosa* via pilus-driven twitching motility. J. Bacteriol. **187:**5560–5567.
33. **Merz, A. J., C. A. Enns, and M. So.** 1999. Type IV pili of pathogenic neisseriae elicit cortical plaque formation in epithelial cells. Mol. Microbiol. **32:**1316–1332.
34. **Merz, A. J., and K. T. Forest.** 2002. Bacterial surface motility: slime trails, grappling hooks and nozzles. Curr. Biol. **12:**R297–R303.
35. **Merz, A. J., D. B. Rifenbery, C. G. Arvidson, and M. So.** 1996. Traversal of a polarized epithelium by pathogenic Neisseriae: facilitation by type IV pili and maintenance of epithelial barrier function. Mol. Med. **2:**745–754.
36. **Merz, A. J., and M. So.** 1997. Attachment of piliated, Opa^- and Opc^- gonococci and meningococci to epithelial cells elicits cortical actin rearrangements and clustering of tyrosine-phosphorylated proteins. Infect. Immun. **65:**4341–4349.
37. **Merz, A. J., and M. So.** 2000. Interactions of pathogenic neisseriae with epithelial cell membranes. Annu. Rev. Cell Dev. Biol. **16:**423–457.
38. **Merz, A. J., M. So, and M. P. Sheetz.** 2000. Pilus retraction powers bacterial twitching motility. Nature **407:**98–102.
39. **Morales, P., P. Reyes, M. Vargas, M. Rios, M. Imarai, H. Cardenas, H. Croxatto, P. Orihuela, R. Vargas, J. Fuhrer, J. E. Heckels, M. Christodoulides, and L. Velasquez.** 2006. Infection of human fallopian tube epithelial cells with *Neisseria gonorrhoeae* protects cells from tumor necrosis factor alpha-induced apoptosis. Infect. Immun. **74:**3643–3650.
40. **Mosleh, I. M., H. J. Boxberger, M. J. Sessler, and T. F. Meyer.** 1997. Experimental infection of native human ureteral tissue with *Neisseria gonorrhoeae*: adhesion, invasion, intracellular fate, exocytosis, and passage through a stratified epithelium. Infect. Immun. **65:**3391–3398.
41. **Nukui, M., T. Shimizu, and Y. Okada.** 2006. Normotonic cell shrinkage induced by Na^+ deprivation results in apoptotic cell death in human epithelial HeLa cells. J. Physiol. Sci. **5:**335–339.
42. **Pena, F. J., F. Saravia, A. Johannisson, M. Walgren, and H. Rodriguez-Martinez.** 2005. A new and simple method to evaluate early membrane changes in frozen-thawed boar spermatozoa. Int. J. Androl. **28:**107–114.
43. **Perdigao, J., P. Lambrechts, B. Van Meerbeek, G. Vanherle, and A. L. Lopes.** 1995. Field emission SEM comparison of four postfixation drying techniques for human dentin. J. Biomed. Mater. Res. **29:**1111–1120.
44. **Pollard, T. D., and G. G. Borisy.** 2003. Cellular motility driven by assembly and disassembly of actin filaments. Cell **112:**453–465.
45. **Pujol, C., E. Eugene, M. Marceau, and X. Nassif.** 1999. The meningococcal PilT protein is required for induction of intimate attachment to epithelial cells following pilus-mediated adhesion. Proc. Natl. Acad. Sci. USA **96:**4017–4022.
46. **Raucher, D., and M. P. Sheetz.** 2000. Cell spreading and lamellipodial extension rate is regulated by membrane tension. J. Cell Biol. **148:**127–136.
47. **Schneider, H., A. S. Cross, R. A. Kuschner, D. N. Taylor, J. C. Sadoff, J. W. Boslego, and C. D. Deal.** 1995. Experimental human gonococcal urethritis: 250 *Neisseria gonorrhoeae* MS11mkC are infective. J. Infect. Dis. **172:**180–185.
48. **Segal, E., P. Hagblom, H. S. Seifert, and M. So.** 1986. Antigenic variation of gonococcal pilus involves assembly of separated silent gene segments. Proc. Natl. Acad. Sci. USA **83:**2177–2181.
49. **Simons, M. P., W. M. Nauseef, T. S. Griffith, and M. A. Apicella.** 2006. *Neisseria gonorrhoeae* delays the onset of apoptosis in polymorphonuclear leukocytes. Cell. Microbiol. **11:**1780–1790.
50. **Skerker, J. M., and H. C. Berg.** 2001. Direct observation of extension and retraction of type IV pili. Proc. Natl. Acad. Sci. USA **98:**6901–6904.
51. **Small, J. V., and G. P. Resch.** 2005. The comings and goings of actin: coupling protrusion and retraction in cell motility. Curr. Opin. Cell Biol. **17:**517–523.
52. **Stephens, D. S.** 1989. Gonococcal and meningococcal pathogenesis as defined by human cell, cell culture, and organ culture assays. Clin. Microbiol. Rev. **2:**S104–S111.
53. **Stephens, D. S., L. H. Hoffman, and Z. A. McGee.** 1983. Interaction of *Neisseria meningitidis* with human nasopharyngeal mucosa: attachment and entry into columnar epithelial cells. J. Infect. Dis. **148:**369–376.

54. **Strom, M. S., and S. Lory.** 1993. Structure-function and biogenesis of the type IV pili. Annu. Rev. Microbiol. **47:**565–596.
55. **van Engeland, M., F. C. Ramaekers, B. Schutte, and C. P. Reutelingsperger.** 1996. A novel assay to measure loss of plasma membrane asymmetry during apoptosis of adherent cells in culture. Cytometry **24:**131–139.
56. **Varga, J. J., V. Nguyen, D. K. O'Brien, K. Rodgers, R. A. Walker, and S. B. Melville.** 2006. Type IV pili-dependent gliding motility in the Gram-positive pathogen *Clostridium perfringens* and other Clostridia. Mol. Microbiol. **62:** 680–694.
57. **Vlachou, D., T. Schlegelmilch, E. Runn, A. Mendes, and F. C. Kafatos.** 2006. The developmental migration of *Plasmodium* in mosquitoes. Curr. Opin. Genet. Dev. **16:**384–391.
58. **Wang, N., J. P. Butler, and D. E. Ingber.** 1993. Mechanotransduction across the cell surface and through the cytoskeleton. Science **260:**1124–1127.
59. **Ward, M. E., and P. J. Watt.** 1972. Adherence of *Neisseria gonorrhoeae* to urethral mucosal cells: an electron-microscopic study of human gonorrhea. J. Infect. Dis. **126:**601–605.
60. **Wolfgang, M., P. Lauer, H. S. Park, L. Brossay, J. Hebert, and M. Koomey.** 1998. PilT mutations lead to simultaneous defects in competence for natural transformation and twitching motility in piliated *Neisseria gonorrhoeae*. Mol. Microbiol. **29:**321–330.
61. **Wolfgang, M., J. P. van Putten, S. F. Hayes, D. Dorward, and M. Koomey.** 2000. Components and dynamics of fiber formation define a ubiquitous biogenesis pathway for bacterial pili. EMBO J. **19:**6408–6418.

Editor: R. P. Morrison